Chinese Chemical Letters 32 (2021) 745–749

Contents lists available at ScienceDirect

Chinese Chemical Letters

journal homepage: www.elsevier.com/locate/cclet

Communication

# Effect of doping order on metal-free heteroatoms dual-doped carbon as oxygen reduction electrocatalyst

Hui-Juan Zhang[a,b,*], Jing Geng[a], Chunlei Cai[a], Zi-Feng Ma[c], Zhong Ma[d], Wenli Yao[e], Junhe Yang[a]

[a] School of Materials Science and Engineering, University of Shanghai for Science and Technology, Shanghai 200093, China
[b] Department of Chemical and Biomolecular Engineering, University of Illinois at Urbana-Champaign, Urbana, Illinois 61801, United States
[c] Department of Chemical Engineering, Shanghai Jiaotong University, Shanghai 200240, China
[d] Department of Chemical Engineering, Waterloo Institute for Nanotechnology (WIN), University of Waterloo, Waterloo, Ontario N2L3G1, Canada
[e] Jiangxi Key Laboratory of Power Battery and Material, Faculty of Materials Metallurgy and Chemistry, Jiangxi University of Science and Technology, Ganzhou 341000, China

ARTICLE INFO

*Article history:*
Received 8 March 2020
Received in revised form 6 April 2020
Accepted 16 April 2020
Available online 11 May 2020

*Keywords:*
Oxygen reduction reaction
Metal-free electrocatalyst
Heteroatoms dual-doped carbon
Doping order
N, P, S and F

ABSTRACT

Metal-free heteroatoms dual-doped carbon has been recognized as one of the most promising Pt/C-substitutes for oxygen reduction reaction (ORR). Herein, we optimize the preparation process by doping order of metal-free heteroatoms to obtain the best electrocatalytic performance through three types of dual-doped carbon, including XC-N (first X doping then N doping), NC-X (first N doping then X doping) and NXC (N and X doping) (X = P, S and F). XC-N has more defect than the other two indicated by Raman spectra. X-ray photoelectron spectrom (XPS) measurements indicate that N and X have been dual-doped into the carbon matrix with different doping contents and modes. Electrocatalytic results, including the potential of ORR peak ($E_p$), the half-wave potential, the diffusion-limiting current density mainly follows the order of XC-N > NC-X > NXC. Furthermore, the synergistic effect of second atom doping are also compared with the single doped carbon (NC, PC, SC and FC). The differences in electronegativity and atomic radius of these metal-free heteroatoms can affect the defect degree, the doping content and mode of heteroatoms on carbon matrix, induce polarization effect and space effect to affect $O_2$ adsorption and product desorption, ultimately to the ORR electrocatalytic performance.


Owing to the zero-emission and high-efficiency, fuel cells have been receiving much attention as clean energy conversion systems. Their performances are significantly governed by the cathode oxygen reduction reaction (ORR), which is in a sluggish reaction kinetics with multi-electron transfer [1–4]. So far, carbon supported precious metal platinum (Pt/C) are still the most efficient ORR electrocatalysts. However, these elelctrocatalysts always suffer from several drawbacks, such as high cost with scarcity, poor stability, low methanol tolerance. To solve these problems, extensive efforts have been made to develop non-precious metals or even metal-free ORR electrocatalysts [1–5].

In 2009, Dai's group first reported that vertically aligned nitrogen-containing carbon nanotubes (VA-NCNTs) can use as a metal-free electrocatalyst with a better ORR electrocatalytic activity, long-term stability and tolerance to crossover effect than Pt/C in alkaline fuel cells [6]. Since then, heteroatom nitrogen-doped carbon nanomaterials, such as carbon nanotubes, graphene and carbon blacks, have been widely studied and considered as the promising metal-free ORR electrocatalysts [6–10]. For example, a three-dimensional nitrogen-doped carbon nanotubes/graphene (3D NCNTs/G) was prepared by pyrolysis of pyridine over a graphene-sheet-supported Ni and displayed a higher ORR activity and selectivity in alkaline electrolyte compared with undoped CNTs/G [7]. It was believed that the different electronegativities between the heteroatom N (3.04) and the C atom (2.55) can break the electroneutrality of adjacent carbon atoms to create positive/negative charged sites, which were favorable for $O_2$ adsorption and charge transfer in the ORR process [6].

With this knowledge in mind, some researchers recently have also found that co-doping of N with other metal-free heteroatoms, such as P, S and F, into carbon materials can further improve the electrocatalytic activity of N single-doped carbon materials for the ORR [11–27]. This situation is mainly attributed to the synergistic

* Corresponding author at: School of Materials Science and Engineering, University of Shanghai for Science and Technology, Shanghai 200093, China.
*E-mail address:* hjzhang@usst.edu.cn (H.-J. Zhang).

https://doi.org/10.1016/j.cclet.2020.05.002
1001-8417/

effect that arises from the other heteroatoms, resulting in a larger asymmetrical spin and higher charge density than that achieved by N single heteroatom doping [11–20]. For instance, Xing's group has found that the incorporation of sulfur into nitrogen-doped carbon (S-NC) can dramatically improve the selectivity of ORR to $H_2O$ than NC [18]. They also revealed that S-doping can reduce the energy barrier of the $O_{2(ads)}$ hydrogenation to form $OOH_{(ads)}$, leading to enhanced intrinsic activity by theoretical research [18]. Considering the highest electronegativity and the smallest atomic radius of F. Zhang and coworkers have prepared NFC electrocatalysts from a melamine hydrogen flouride salt and found an obvious synergistic effect from N and F [16]. Hu's group has compared two kinds of B and N dual-doped carbon nanotubes dominated by bonded or separated B and N, and found that the separated one had better ORR electrocatalysts by the experimental and theoretical results [20]. Xia's group predicted the synergistic effect of co-doping occurs within a certain distance between each dopant and pointed out several design principles [28]. Here, we are very curious about whether there is any doping order effect of these heteroatoms for metal-free co-doepd carbon electrocatalysts?

On the basis of the differences in electronegativity between metal-free heteroatoms (N: 3.04, P: 2.19, S: 2.58, F: 3.98) and carbon atom (C: 2.55) as well as atomic radius of metal-free elements (N: 0.075 nm, P: 0.110 nm, S: 0.102 nm, F: 0.071 nm) and carbon atom (C: 0.077 nm) in the elemental periodic table as shown in Fig. S1a (Supporting information), in this study, we choose several heteroatoms, P, S and F, to understand the doping order effect on metal-free heteroatoms dual-doped carbon as ORR electrocatalysts, althogh many attention has been focused on dual-doped of metal-free heteroatoms on carbon nanomaterials [11–20].

In view of the different electronegativity and atomic radius of metal-free elements N, P, S and F, as shown in Fig. S1a, we here design multiple parallel experiments in order to understand the effect of metal-free heteroatoms doping order on the structure and electrocatalytic performance of dual-doped carbon electrocatalysts. The detail description of these multiple parallel experiments are as follows.

0.2 g carbon black and 0.2 g X-acid (phosphoric acid, sulphuric acid and hydrofluoric acid, respectively) were mixed in 2 mL deionized water. The resulting powder was then pyrolyzed at 800 °C for 90 min with a heating rate of 5 °C/min in $N_2$ atmosphere. After cooling down to room temperature, this sample was named as XC and mixed with 0.2 g melamine, then pyrolyzed again at 800 °C for 90 min with a heating rate of 5 °C/min in $N_2$ atmosphere. After cooling down to room temperature, metal-free XC-N were obtained.

0.2 g carbon black and 0.2 g melamine were mixed thoroughly. The resulting powder was then pyrolyzed at 800 °C for 90 min with a heating rate of 5 °C/min in $N_2$ atmosphere. After cooling down to room temperature, this sample was named as NC and mixed with 0.2 g X-acid in 2 mL deionized water, then the resulting powder pyrolyzed again at 800 °C for 90 min with a heating rate of 5 °C/min in $N_2$ atmosphere.

0.2 g carbon black, 0.2 g melamine and 0.2 g X-acid were mixed in 2 mL deionized water. The resulting powder was then pyrolyzed at 800 °C for 90 min with a heating rate of 5 °C/min in $N_2$ atmosphere. In order to be comparable with the above-mentioned samples (XC-N and NC-X), it was pyrolyzed again at 800 °C for 90 min with a heating rate of 5 °C/min in $N_2$ atmosphere. In this way, metal-free NXC were obtained.

Raman spectra of these metal-free electrocatalysts were recorded from 700 $cm^{-1}$ to 2000 $cm^{-1}$ at room temperature on a LabRAM HR Evolution equipped with a 532 nm laser excitation. The spectra data were analyzed by fitting with four symmetric peaks using Lorentzian function: D peak (1340–1355 $cm^{-1}$), G peak (1580–1600 $cm^{-1}$), Am peak (1490–1525 $cm^{-1}$) and P peak (1150–1190 $cm^{-1}$) [29–31]. X-ray photoelectron spectra (XPS) were carried out on a PERKIN ELMZR PHI 3056 with an Al K$\alpha$ monochromated. The spectra position of N and X (X = P, S and F) were calibrated from C = 284.8 eV and corrected for the background using the Shirley approach in the XPSPeak4.1 software.

Electrochemical measurements, such as cyclic voltammograms (CVs), rotating disk electrode (RDE) and rotating ring-disk electrode (RRDE) measurements, were performed on the CHI 760D in 0.1 mol/L KOH solution at room temperature. The electrocatalyst ink was prepared by ultrasonically dispersing 5 mg electrocatalyst powder in 950 μL anhydrous ethanol and 50 μL 5 wt% Nafion solution for 30 min. 20 μL of this ink was deposited onto the surface of a RRDE (d = 5.61 mm) and air-dried for further use. A conventional three-electrode system, including a graphite rode, a saturated calomel electrode (SCE) and the electrocatalyst-coated RRDE were used as the counter electrode, the reference electrode and the working electrode, respectively. The potential scan range was set between -0.8 V and 0.2 V at a fixed potential scan rate of 5 mV/s. CVs were first collected in $N_2$-saturated solution to obtain the background capacitive currents, then CVs were recorded in $O_2$-saturated solution for the electrocatalytic ORR. The disk currents and the ring currents were recorded at a rotation rate of 900 rpm, furthermore, the disk potential was maintained at 0.5 V for the ring currents.

Raman spectroscopy is the most effective and non-destructive technique to characterize the structure of carbon materials, in particular to determine defects and disordered structures. Fig. 1 shows the Raman spectra of all samples with four distinct fitting peaks, which are D peak (1340 $cm^{-1}$), G peak (1590 $cm^{-1}$), P peak (1150–1190 $cm^{-1}$) and Am peak (1490–1525 $cm^{-1}$), respectively [29–31]. Generally speaking, the D peak relates to a series of lattice defects and disorder degree of carbon atoms, such as bond angle disorder, bond length disorder, as well as hybridization; whereas the G peak arises from the in-plane stretching vibration of $sp^2$-hybridized carbon atoms [16,30,32]. Here, we take three parameters to assess the defect degree of these dual-doped carbon comprehensively: The intensity ratio ($I_D/I_G$), the area ratio ($A_D/A_G$) and the full width at half maximum ratio ($W_D/W_G$) of the D peak and G peak. These obtained parameters are listed and compared in Table S1 (Supporting information). Specially, for NC–P, NPC and PC–N, they are (1) PC–N (2.10) > NC–P (2.07) > NPC (2.04), (2) PC–N (2.61) > NPC (2.43) > NC–P (2.24) and (3) PC–N (1.25) > NPC (1.20) > NC–P (1.10) for $W_D/W_G$, $A_D/A_G$ and $I_D/I_G$, respectively, meaning that PC–N has the most disorder and the largest defect degree. For NC–S, NSC and SC-N, they are (1) SC-N (2.42) > NSC (2.27) > NC-S (2.25), (2) SC-N (3.20) > NSC (3.18) > NC–S (2.81) and (3) SC–N (1.42) > NSC (1.33) > NC-S (1.27) for $W_D/W_G$, $A_D/A_G$ and $I_D/I_G$, respectively, demonstrating that SC–N has the most disorder and the highest defect degree. For NC–F, NFC and FC–N, they are (1) FC–N (2.18) > NFC (2.09) > NC–F (2.03), (2) FC–N (2.72) > NFC (2.66) > NC–F (2.47) and (3) FC-N (1.30) > NFC (1.22) = NC–F (1.22) for $W_D/W_G$, $A_D/A_G$ and $I_D/I_G$, respectively, showing that FC-N has the most disorder and the highest defect degree. This clearly implies that among these dual-doped carbon materials, the XC-N (X = P, S, F) has the highest defect degree than the other two components (NXC and NC-X).

The doping content and mode of metal-free heteroatoms N, P, S and F on carbon are measured and analyzed by XPS. Quantitative results of doping content are displayed in Table S2 (Supporting information), indicating that N and metal-free heteroatoms (P, S and F) have been successfully dual-doped into the carbon matrix. The atomic contents of N are 1.26, 1.75 and 1.52 for NC-P, NPC and PC-N, 1.41, 2.43 and 0.98 for NC-S, NSC and SC-N, 0.84, 1.09 and 0.82 for NC-F, NFC and FC-N, respectively. Fig. 2 shows the high resolution N 1s spectra of these samples. Each one is mainly

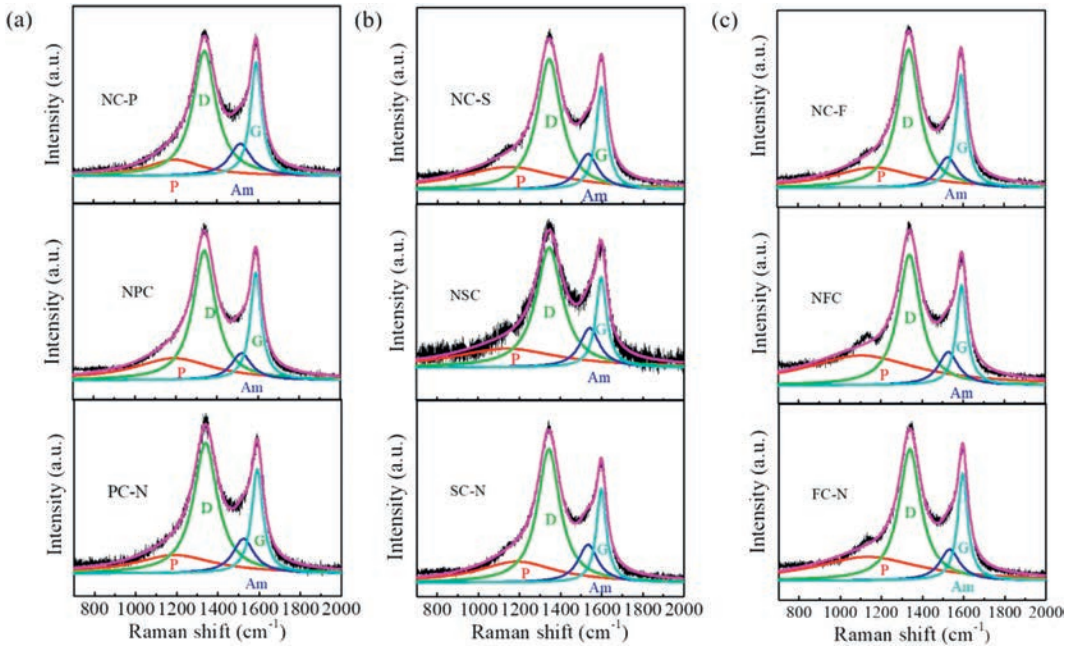


**Fig. 1.** Raman spectra with four fitting peaks (D peak, G peak, P peak and Am peak) of (a) NC-P, NPC and PC-N; (b) NC-S, NSC and SC-N; and (c) NC-F, NFC and FC-N.

deconvoluted into three types: pyridinic N (~398.4 eV), pyrrolic N (~399.9 eV) and graphitic N (~401.3 eV), which are typically observed in N-doped carbon [16,30,32–34]. Graphitic N corresponds to N atoms that are doped into carbon matrix by substitution the carbon atoms in hexagonal ring, while pyrrolic N refers to having two p electrons and p-conjugated bond system of N atoms and pyridinic N refers to the N atom in N-doped carbon surface on the edge of two carbons. Furthermore, the percentage of each component is about 30% as listed in Table S2.

The atomic contents of P are 0.43%, 1.12% and 0.46% for NC-P, NPC and PC-N, respectively. The high resolution P 2p spectra in Fig. S2a (Supporting information) is deconvoluted into two different signals at about 133 eV and 134 eV with binding energies analogous to $2p_{3/2}$ and $2p_{1/2}$, respectively. The P 2p at 133 eV is attributed to the P-C coordination, which is favorable for oxygen molecule adsorption and 134 eV is the P—O bonding [31,35,36]. For NC–S, NSC and SC–N, the S content on carbon are 0.15%, 0.07% and 0.20%, respectively. Fig. S2b (Supporting information) shows the high resolution S 2p spectra of these samples. In the high resolution S 2p spectra, it consists of two components at about 164 eV and 165 eV, which originate from the $2p_{3/2}$ and $2p_{1/2}$ of thiophene-S owing to their spin-orbit coupling, respectively [33,35]. These two major peaks are attributed to the sulfur binding in C–S–C bond and conjugated -C = S- bond, respectively [31,26–

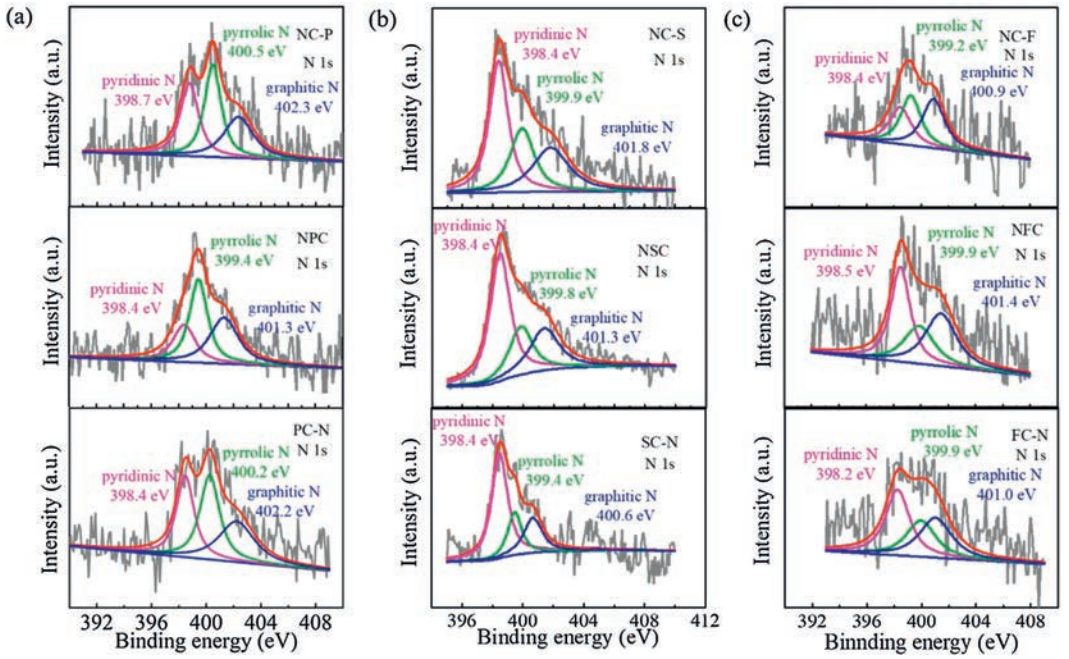


**Fig. 2.** High resolution XPS spectra of N 1s in (a) NC-P, NPC and PC-N; (b) NC-S, NSC and SC-N; and (c) NC-F, NFC and FC-N.

30]. These C–S–C and –C=S– species have some contributors to ORR activity [31]. Besides, the third peak at the binding energy of around 168.8 eV for the SC-N is from oxidized sulfur (—$SO_n$—) [34,36,37]. The high resolution F 1s spectra of these samples are given in Fig. S2c (Supporting information). Two components attributing to the ionic C—F bond and semi-ionic C—F bond can be deconvoluted, respectively [12,16].

The electrocatalytic performances of CVs for XC-N, NC-X and NXC (X = P, S and F) are compared and shown in Fig. 3. The CVs in $N_2$-saturated (dotted line) 0.1 mol/L KOH solution are featureless (no peak) for all samples, in contrast, a single well-defined ORR peak can be obtained in $O_2$-saturated (solid line) solution for each one. In Fig. 3a, the potential of ORR peak ($E_p$) shifts positively as the order of PC-N (784 mV) > NC-P (755 mV) > NPC (751 mV). The $E_p$ follows the order of SC-N (783 mV) > NC-S (764 mV) > NSC (754 mV) in Fig. 3b and FC-N (788 mV) > NC-F (773 mV) > NFC (759 mV) in Fig. 3c. This means that XC-N has better electrocatalytic performances than NXC and NC-X (X = P, S and F).

To further investigate the electrocatalytic performances of XC-N, NC-X and NXC (X = P, S and F), RDE and RRDE measurements are both conducted and compared in Fig. 4. For the current-potential curves of the disk electrode in $O_2$-saturated 0.1 mol/L KOH solution (at the bottom of Fig. 4, a S-shaped curve for each sample is clearly displayed. Moreover, a more positive half-wave potential and a higher diffusion-limiting current density is generally occurred on XC-N, especially SC-N and FC-N, which is better than the other two types. For example, at the current density of 2 mA/cm$^2$, SC-N has a half-wave potential of 740 mV, better than NC-S (677 mV) and NSC (695 mV) and FC-N has a half-wave potential of 764 mV, better than NC-F (727 mV) and NFC (718 mV). The ring currents as a function of the disk potential (at the top of Fig. 4) initiate simultaneously as the disk currents, indicating the generation of peroxide is taking place. Furthermore, the ring currents increase as the disk potential decrease, appearing an ring current-disk potential dependent.

There are two parallel reaction mechanisms for ORR in solution: One is the 2-electron path accompanied with the peroxide product and the other is 4-electron path. Based on Eq. S2 (Supporting information), the number of electrons transferred per molecule oxygen (n) are calculated and displayed in Fig. S3 (Supporting information). On the whole, the n of all these samples are more than 2.0 but less than 4.0, meaning the ORR on each sample is conducted in a mixed reaction of 2-electron and 4-electron. Moreover, the n of these samples are all more than 3.0, meaning that the ORR on these electrocatalysts is in a predominant 4-electron path. Concretely, the n on PC-N and NC-P are more than 3.4 and larger than that of NPC, indicating that the ORR electrocatalytic 4-electron selectivity order is NC-P > PC-N > NPC (Fig. S3a). SC-N has an n more than 3.5 and are much larger than that of NSC and NC-S, indicating a better ORR electrocatalytic 4-electron selectivity of SC-N (Fig. S3b). The n on FC-N and NC-F are larger than that of NFC, indicating that the ORR electrocatalytic 4-electron selectivity order is NC–F > FC–N > NFC (Fig. S3c).

To further investigate the ORR electrocatalytic reaction mechanism of XC-N, NC-X and NXC (X = P, S and F), the percentage of peroxide (peroxide%) are calculated according to Eq. S3 (Supporting information) and shown in Fig. S4 (Supporting information), accordingly. Overall, the peroxide% is lower than 50% for each one, further meaning that the ORR on these electrocatalysts is a mixed 2-electron and 4-electron reaction. For example, the peroxide% of PC-N and NC-P are less than 30 % and less than that of NPC, further indicating that the ORR electrocatalytic 4-electron selectivity order is NC-P > PC-N > NPC (Fig. S4a). SC-N has a peroxide% less than 20% and are much less than that of NSC and NC-S, indicating a better ORR electrocatalytic 4-electron selectivity of SC-N (Fig. S4b).

To further understand the synergistic effect of second atom doping, we also prepared the single doped carbon, namely NC, PC, SC and FC. Fig. S5 (Supporting information) show their typical CVs and the disk current densities in $O_2$-saturated 0.1 mol/L KOH solution, respectively. We can see an order of NC (790 mV) > PC (772 mV) > SC (762 mV) > FC (753 mV) on the term of the ORR peak potential. These electrocatalytic activities are all lower than that of metal-free heteroatoms dual-doped carbon (Fig. 3). The polarization curves of single-doped carbon in Fig. S5b demonstrate two-step platforms, indicating a two-electron reaction pathway on these electrocatalysts. Furthermore, half-wave potentials of 732 mV, 739 mV, 694 mV and 705 mV are for NC, PC, SC and FC, respectively, which are more negative than dual-doped carbon (Fig. 4). These also verify the synergistic effect of second atom doping.

Here, we know that the electrocatalytic performance, including the potential of ORR peak ($E_p$), the half-wave potential and the diffusion-limiting current density mainly follows the order of XC-N > NC-X > NXC (X = P, S and F). Combining with the fact that the electronegativity of these metal-free heteroatoms is F (3.98) > N (3.04) > S (2.58) > C (2.55) > P (2.19) and atomic radius of these metal-free heteroatoms is P (0.110 nm) > S (0.102 nm) > C (0.077 nm) > N (0.075 nm) > F (0.071 nm), here we can believe that the different doping order of these metal-free heteroatoms can induce polarization effect and space effect to affect $O_2$ adsorption and product desorption, ultimately to affect the ORR electrocatalytic performance. Lei *et al*. has also pointed out the space confinement and vacancy defect of N-doped carbon on the ORR electrocatalytic activity [31]. The different doping order of these metal-free heteroatoms can also generate different defect degree along with different doping contents and modes.

In summary, we have reported a rational doping order of metal-free heteroatoms to obtain the best electrocatalytic performance through three types of dual-doped carbon, including XC-N, NC-X and NXC (X = P, S and F). Electrocatalytic results, including the potential of ORR peak ($E_p$), the half-wave potential, the diffusion-limiting current density mainly follows the order of XC-N > NC-X > NXC. Furthermore, the synergistic effect of second atom doping are also appeared compared with the single doped carbon (NC, PC, SC and FC). The different doping order of these metal-free heteroatoms can

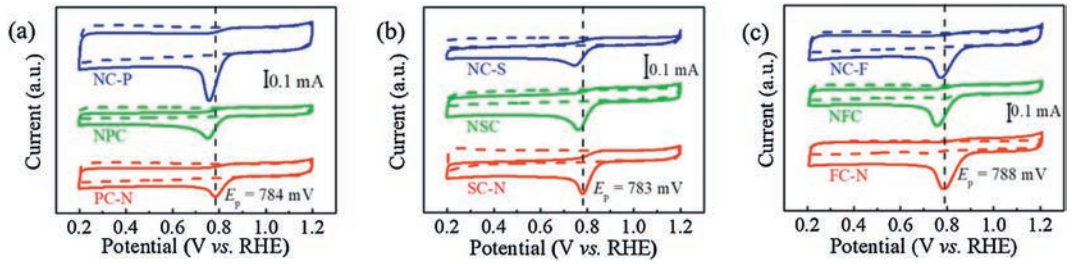


**Fig. 3.** Typical CVs of (a) NC-P, NPC and PC-N; (b) NC-S, NSC and SC-N; and (c) NC-F, NFC and FC-N in $O_2$-saturated 0.1 mol/L KOH solution.

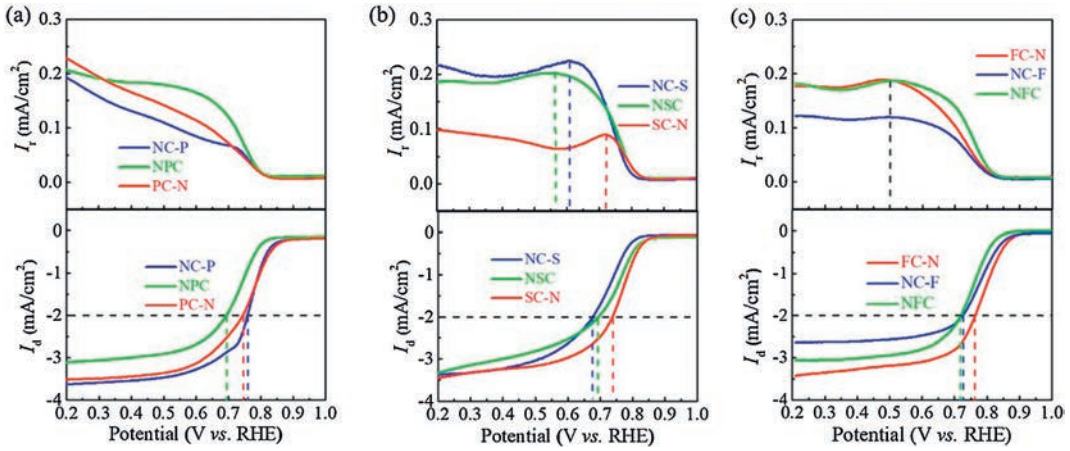


**Fig. 4.** The disk current densities ($I_d$) and the ring current densities ($I_r$) of (a) NC-P, NPC and PC-N; (b) NC-S, NSC and SC-N; and (c) NC-F, NFC and FC-N in $O_2$-saturated 0.1 mol/L KOH solution.

also generate different defect degree along with different doping contents and modes. Raman spectra indicate XC-N has more defect than the other two. N and X have been dual-doped into the carbon matrix with different doping contents and modes measured by XPS measurements. Combining with the differences in electronegativity and atomic radius of these metal-free heteroatoms, here we can believe that the different doping order of these metal-free heteroatoms can induce polarization effect and space effect to affect $O_2$ adsorption and product desorption, ultimately to the ORR electrocatalytic performance.

## Declaration of competing interest

There are no conflicts to declare.

## Acknowledgments

The authors are grateful for the financial support of this work by the National Natural Science Foundation of China (No. 21406139), the Development Project of University of Shanghai for Science and Technology (No. 2019KJFZ019), the Scientific Research Innovation Project of Shanghai Education Commission (No. 2019-01-07-00-07-E00015), and the Basic Research Project (No. 19JC1410402).

## Appendix A. Supplementary data

Supplementary material related to this article can be found, in the online version, at doi:https://doi.org/10.1016/j.cclet.2020.05.002.

## References

[1] Y. Nie, L. Li, Z.D. Wei, Chem. Soc. Rev. 44 (2015) 2168–2201.
[2] D.G. Li, H.F. Lv, Y.J. Kang, N.M. Markovic, V.R. Stamenkovic, Annu. Rev. Chem. Biomol. 7 (2016) 509–532.
[3] J. Wang, Z.D. Wei, Acta. Phys-Chim. Sin. 33 (2017) 886–902.
[4] X.Q. Wang, Z.J. Li, Y.T. Qu, et al., Chemistry 5 (2019) 1486–1511.
[5] H.J. Zhang, X.X. Yuan, W. Wen, et al., Electrochem. Commun. 11 (2009) 206–208.
[6] K.P. Gong, F. Du, Z.H. Xia, M. Durstock, L.M. Dai, Science 323 (2009) 760–764.
[7] Y.W. Ma, L.Y. Sun, W. Huang, et al., J. Phys. Chem. C 115 (2011) 24592–24597.
[8] N. Brun, S.A. Wohlgemuth, P. Osiceanu, M.M. Titirici, Green Chem. 15 (2013) 2514–2524.
[9] G. Nam, J. Park, S.T. Kim, et al., Nano Lett. 14 (2014) 1870–1876.
[10] H.W. Liang, Z.Y. Wu, L.F. Chen, C. Li, S.H. Yu, Nano Energy 11 (2015) 366–376.
[11] C. Han, X.J. Bo, Y.F. Zhang, M.A. Li, L.P. Guo, J. Power Sources 272 (2014) 267–276.
[12] H.J. Zhang, X. Zhang, S.W. Yao, et al., J. Electrochem. Soc. 164 (2017) H1081–H1085.
[13] T.V. Vineesh, M.A. Nazrullaa, S. Krishnamoorthy, T.N. Narayanan, S. Alwarappan, Appl. Mater. Today 1 (2015) 74–79.
[14] J. Geng, H.J. Zhang, S.W. Yao, et al., RSC Adv. 9 (2019) 24770–24776.
[15] Y.N. Sun, M.L. Zhang, L. Zhao, et al., Adv. Mater. Interf. 6 (2019) 1–9.
[16] H.J. Zhang, S.W. Yao, J. Geng, Z.F. Ma, J.H. Yang, J. Colloid Interface Sci. 535 (2019) 436–443.
[17] J. Gao, N. Ma, J.J. Tian, et al., J. Solid State Electr. 22 (2018) 519–525.
[18] J.B. Zhu, K. Li, M.L. Xiao, et al., J. Mater. Chem. A 4 (2016) 7422–7429.
[19] J.M. Chabu, L.Q. Wang, F.Y. Tang, et al., Chemelectrochem 4 (2017) 1885–1890.
[20] Y. Zhao, L.J. Yang, S. Chen, et al., J. Am. Chem. Soc. 135 (2013) 1201–1204.
[21] C.E. Zhao, J.X. Li, Y. Chen, J.Y. Chen, New J. Chem. 43 (2019) 9389–9395.
[22] Y.P. Xie, Y. Yang, Q.J. Zhou, et al., J. Electrochem. Soc. 166 (2019) H549–H555.
[23] S.T. Yang, X.X. Mao, Z.X. Cao, et al., Appl. Surf. Sci. 427 (2018) 626–634.
[24] T. Sun, J. Wang, C.T. Qiu, et al., Adv. Sci. 5 (2018) 1–9.
[25] Y. Lv, X.B. Wang, T. Mei, J.H. Li, J.Y. Wang, ChemistrySelect 3 (2018) 3241–3250.
[26] Z.P. Zhang, J.T. Sun, M.L. Dou, J. Jo, F. Wang, ACS Appl. Mater. Interfaces 9 (2017) 16236–16242.
[27] M.B. Wu, Y. Liu, Y.L. Zhu, et al., J. Mater. Chem. A 5 (2017) 11331–11339.
[28] Z.H. Zhao, Z.H. Xia, ACS Catal. 6 (2016) 1553–1558.
[29] F. Jaouen, F. Charreteur, J.P. Dodelet, J. Electrochem. Soc. 153 (2006) A689–A698.
[30] H.L. Li, H.J. Zhang, X.T. Li, et al., Int. J. Hydrogen Energy 39 (2014) 3198–3210.
[31] Y.X. Zan, Z.P. Zhang, M.L. Dou, F. Wang, Catal. Sci. Technol. 9 (2019) 5906–5914.
[32] Z.F. Yang, J.X. Han, R. Jiao, et al., A. Li, J. Colloid Interf. Sci. 557 (2019) 664–672.
[33] Z. Liu, H.G. Nie, Z. Yang, et al., Nanoscale 5 (2013) 3283–3288.
[34] X. Wang, J. Wang, D.L. Wang, et al., Chem. Commun. 50 (2014) 4839–4842.
[35] S.S. Shinde, C.H. Lee, A. Sami, et al., ACS Nano 11 (2017) 347–357.
[36] Y.N. Zhu, C.Y. Cao, W.J. Jiang, et al., J. Mater. Chem. A 4 (2016) 18470–18477.
[37] Z.X. Wu, R. Liu, J. Wang, et al., Nanoscale 8 (2016) 19086–19092.